

Transit Clairvoyance: Enhancing TESS follow-up using artificial neural networks

David M. Kipping^{1*} and Christopher Lam¹

¹*Dept. of Astronomy, Columbia University, 550 W 120th Street, New York NY 10027*

Accepted . Received ; in original form

ABSTRACT

The upcoming *TESS* mission is expected to find thousands of transiting planets around bright stars, yet for three-quarters of the fields observed the temporal coverage will limit discoveries to planets with orbital periods below 13.7 days. From the *Kepler* catalog, the mean probability of these short-period transiting planets having additional longer period transitors (which would be missed by *TESS*) is 18%, a value ten times higher than the average star. In this work, we show how this probability is not uniform but functionally dependent upon the properties of the observed short-period transitors, ranging from less than 1% up to over 50%. Using artificial neural networks (ANNs) trained on the *Kepler* catalog and making careful feature selection to account for the differing sensitivity of *TESS*, we are able to predict the most likely short-period transitors to be accompanied by additional transitors. Through cross-validation, we predict that a targeted, optimized *TESS* transit and/or radial velocity follow-up program using our trained ANN would have a discovery yield improved by a factor of two. Our work enables a near-optimal follow-up strategy for surveys following *TESS* targets for additional planets, improving the science yield derived from *TESS* and particularly beneficial in the search for habitable-zone transiting worlds.

Key words: eclipses — planets and satellites: detection — methods: numerical — stars: planetary systems

1 INTRODUCTION

In 2013, NASA’s *Kepler Mission* ended its four year vigil of a 100 deg² patch of the sky. The data obtained during this time will likely continue to be a rich vein of scientific discovery for years to come. Whilst the *Kepler* data has certainly revealed remarkable individual discoveries (e.g. Doyle et al. 2011; Kipping & Spiegel 2011; Rappaport et al. 2012; Muirhead et al. 2012), the statistical insights afforded by this homogenous catalog of over four thousand transiting planet candidates have arguably been the most transformative (e.g. see Howard et al. 2012; Dong & Zhu 2013; Petigura et al. 2013; Foreman-Mackey et al. 2014; Dressing & Charbonneau 2015; Burke et al. 2015; Traub 2016).

The next major space-based transit survey will be NASA’s *Transiting Exoplanet Survey Satellite*, or *TESS*, expected to be launched late-2017/early-2018 (Ricker et al. 2015). Unlike *Kepler*, *TESS* will survey a large fraction of the sky, seeking planets around the nearest and brightest stars suitable for detailed subsequent characterization. The *TESS* survey strategy comes at the cost of having to peri-

odically shift fields to tile the sky. This means that during the 2 year nominal mission, more than three-quarters of the *TESS* observed fields will be monitored for just 27.4 days. One major effect of this is that the ability of *TESS* to discover long-period planets is severely diminished compared to that of the *Kepler Mission* (Sullivan et al. 2015).

Despite this, *TESS* is expected to discover ~1700 short-period transiting planets (Sullivan et al. 2015). Thanks to *Kepler*, we know that multiple transiting planet systems are common, comprising ~20% of all observed *Kepler* systems (Coughlin et al. 2016) and thus many of these ostensibly single transiting planet *TESS* systems will in fact have additional, longer-period transiting planets missed by *TESS*. Since only ~2% of *Kepler* targets are observed to host transiting planets but ~20% of these have multiple transiting planets, the ~1700 short-period *TESS* systems are much more likely to be fruitful targets for subsequent transit searches than an average target. Yet even with this advantage, conducting long-term precise photometric monitoring of ~1700 targets dispersed across the entire sky would be non-trivial for ground- and space-based observatories.

In this work, we demonstrate that the probability of a short-period transiting planet(s) (“inner(s)”) harboring an

* E-mail: dkipping@astro.columbia.edu

additional long-period transiting planet(s) (“outer(s)”) is not a single number, but instead is functionally dependent upon the properties of the short-period planet(s). This insight enables us to predict which single transiting planet systems are most likely to be fruitful for subsequent transit follow-up. Applying ideas from machine learning, we train a feed-forward artificial neural network to the observed *Kepler* catalog, which we show can be used to increase the yield of a mock transit follow-up program by a factor of two.

We briefly introduce artificial neural networks and our particular implementation in Section 2. Data preprocessing and training of the network to the *Kepler* sample is discussed in Section 3, including investigations of varying the properties of the network. We extend our model to include an additional feature, yet still account for sensitivity bias, using a hybrid network discussed in Section 4. We discuss the potential applications and physical interpretation of our work in Section 6.

2 ARTIFICIAL NEURAL NETWORKS

Artificial neural networks (ANNs) are a class of machine learning techniques designed to estimate or approximate complex functions, taking inspiration from biological neural networks, such as those found in the brain. An ANN can be considered to be a function composed of many simple processing elements which relate an array of inputs, \mathbf{X} , to an array of outputs, $\hat{\mathbf{Y}}$. In what follows, we consider the case of *supervised* ANNs only.

The t^{th} row of \mathbf{X} is a real-valued vector, x_t , of length equal to the number of different input variables, N , where t is the index of each training example. The different input variables are often called *features*, which together describe the *input pattern* to the network. Similarly, the t^{th} row of $\hat{\mathbf{Y}}$ is the corresponding, real-valued output vector, y_t , of length equal to the number of different output variables, M . The matrix $\hat{\mathbf{Y}}$ is an approximation of the desired output, \mathbf{Y} .

Generally, an ANN is a structure of weighted interconnections between a layer of input neurons, hidden layers of processing neurons and the final layer of output neurons (for example, see Figure 1). The hidden neurons most often perform nonlinear scalar transformations (although they can also be linear), described by their *activation function*, Φ . All inputs to a neuron are multiplied by weights, often called *synaptic strengths*, which are summed together and then transformed via the activation function (Haykin 1994). The structure, number of hidden layers and neurons, as well as the activation functions, are chosen by the user and generally one aims to use the simplest possible network to satisfactorily relate \mathbf{X} to $\hat{\mathbf{Y}}$, in order to avoid over-fitting (Sarle 1995). The synaptic strengths are then fitted to maximize the agreement between $\hat{\mathbf{Y}}$ and \mathbf{Y} .

2.1 Feedforward Multilayer Perceptrons

In this work, we have used one of the most commonly used types of supervised neural networks, that of *multilayer perceptrons*, also commonly referred to as a *feedforward* (FF) network (see Bishop 1995 for an introduction). FF networks have been used in a variety of astronomical applications (for example, see Lundstedt & Wintoft 1994; Snider et al. 2001;

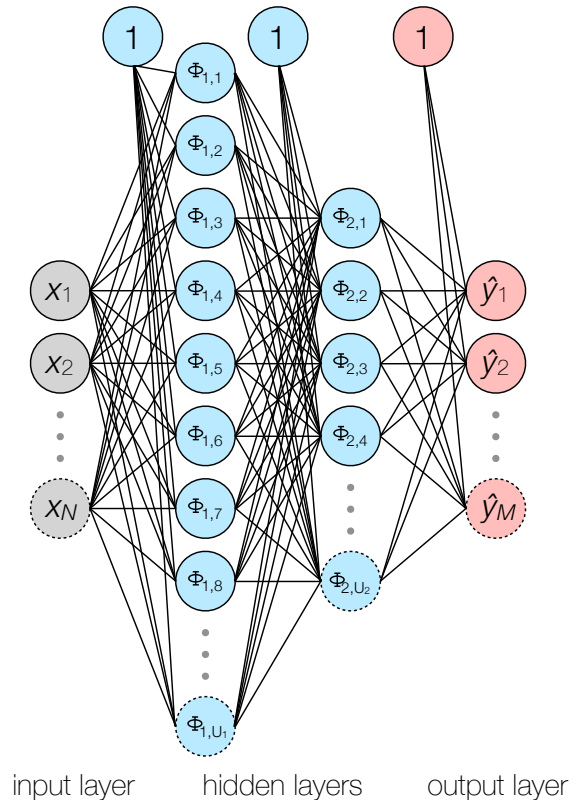


Figure 1. Architecture of a feedforward artificial neural network with two hidden layers. An input pattern, x , is transformed into an output pattern, y , using the synaptic strengths, network structure, bias terms (1’s) and activation functions (Φ).

Vanzella et al. 2004; Graff et al. 2014) and are well-suited for classification problems (Bailer-Jones et al. 2001).

The FF network structure is illustrated in Figure 1, where we depict two hidden layers although any arbitrary number is possible. For each input pattern injected into the network, an output pattern is produced using the *propagation rule*. Each hidden layer neuron is connected to all of the previous layer’s neurons, as well as a bias term, with variable synaptic strengths. The output of the hidden neurons are then computed using the activation functions and fed-forward to the next hidden layer, which follows the same behavior. Whereas the hidden neurons typically use nonlinear activation functions, the output layer is calculated using the weighted sum of the previous layer’s output. In a classification problem, such as our own, this output represents the class probability which may be converted to a binary classification using a logistic sigmoid.

Using this feedforward propagation, we may define the output pattern from the FF network, y , given an input pattern, x . For example, the q^{th} output neuron in a single-layer FF network, \hat{y}_q , will be given by

$$\hat{y}_q = \beta_q + \sum_{k=1}^U v_{q,k} \Phi_k \left[\sum_{j=1}^N b_k + w_{k,j} x_j \right]. \quad (1)$$

The various terms in the above expression can be under-

stood as follows. β_q is the synaptic strength to the output layer bias for the q^{th} output neuron. U is the number of neurons, or units, in the hidden layer. $v_{q,k}$ is the synaptic strength between the q^{th} output neuron and the k^{th} neuron in the hidden layer. Φ_k is the activation function of the k^{th} neuron in the hidden layer. b_k is the synaptic strength between the hidden layer bias and the k^{th} neuron in the hidden layer. $w_{k,j}$ is the synaptic strength between the j^{th} neuron in the input layer of the k^{th} neuron in the hidden layer.

When training a single-layer FF network then, the vector of synaptic strengths to fit, given by $\theta = \{\beta, u, b, w\}$, has a total length of $\dim(\theta) = U + M + NU + UM$.

The above may be extended to more hidden layers, but requires introducing extra notation indices for each layer, which we denote using subscripts. The output of a double-layer FF network may now be expressed as

$$\hat{y}_q = \beta_q + \sum_{k=1}^{U_2} v_{q,k} \Phi_{2,k} \left[\sum_{j=1}^{U_1} b_{2,k} + w_{2,k,j} \Phi_{1,j} \left[\sum_{i=1}^N b_{1,j} + w_{1,j,i} x_i \right] \right]. \quad (2)$$

Here, the total number of synaptic strengths is now $\dim(\theta) = U_1 + U_2 + M + NU_1 + U_1 U_2 + U_2 M$.

2.2 Activation Functions

Whilst several non-linear activation functions are commonly used, the rectifier function is the most popular in deep learning (LeCun et al. 2015), given by

$$\Phi[z] = \max(0, z). \quad (3)$$

Rectifiers are efficient to compute and differentiable (except at zero), yet do not have the vanishing gradient problem afflicting traditional activation functions, such as the hyperbolic function (Hochrieter 1991). For these reasons, we elected to adopt this popular activation function in what follows for all hidden neurons. We describe later how using an alternative activation function does not affect the results of this work.

2.3 Learning Algorithm

In order to determine the synaptic strengths, we need to train the FF network. First then, we must define a cost function to optimize.

In our work, the output layer comprises of a single neuron, which represents the binary classification probability as to whether the input pattern, describing properties of a particular planetary system, has one or more additional transiting planets with periods $P > P_{\text{cut}}$. The typical error function used is the mean square error (MSE), which for our problem is given by

$$\epsilon(\theta) = \frac{1}{T} \sum_{t=1}^T (y_t - \hat{y}_t(\theta))^2, \quad (4)$$

where T is the total number of training examples.

The most commonly used learning techniques for ANNs are back-propagation algorithms, which essentially use some form of gradient descent to optimize the cost function. In

what follows, we elect to use one of the most popular learning methods, the damped least squares Levenberg-Marquardt algorithm (LMA) (Levenberg 1944; Marquardt 1963). We set the LMA to stop once the cost function improves by less than 1 part in 10^8 .

We also update the cost function to include a modest regularization term, using L_2 -regularization. Regularization is frequently used to help ANNs avoid overfitting the training set, pulling the learning back from fitting small noisy spikes and imposing a preference for an overall smoothness to the ANN function. This leads to our final cost function, C , of,

$$C(\theta) = \epsilon(\theta) + \delta \theta^T \theta \quad (5)$$

where δ is the L_2 regularization coefficient. After experimenting with different values, we settled on $\delta = 0.1$ as providing a good balance between flexibility and smoothness. In order to validate the learning, we employ cross-validation and choose an FF network structure using the early stopping principle, both of which we describe later in Section 3.3 & 3.4, respectively.

3 TRAINING DATA

3.1 Training Data

We downloaded the *Kepler* planetary candidates catalog from the NASA Exoplanet Archive (Akeson et al. 2013) on May 17th 2016. Data were filtered such that only objects dispositioned as planetary candidates by *Kepler* were used, giving us 4696 such objects.

We filtered the catalog for radii $R_p < 32 R_{\oplus}$, since objects larger than this are very unlikely to be planets (Chen & Kipping 2016), and $\log g > 4$, since the false positive rate increases sharply beyond this (Sliski & Kipping 2014). These filters reduced our planet sample to 4022 planetary candidates in 3056 systems.

TESS can only strongly constrain the orbital period of planets which are observed to undergo multiple transits. This means that only transiting planets with orbital periods less than $P_{\text{cut}} = B/2$, where B is the baseline of observations, are guaranteed to undergo ≥ 2 transits necessary for a strong orbital period determination. For $\gtrsim 75\%$ of the *TESS* observed fields, $B = 27.4$ d, since overlapping fields near the ecliptic pole allow for greater B (Sullivan et al. 2015). In this work, we adopt $B = 27.4$ d and thus $P_{\text{cut}} = 13.7$ d, although the ANN presented here could be re-trained for other choices of P_{cut} . After removing any systems for which there are no transiting planets with $P < P_{\text{cut}}$, we are left with 1786 systems, each of which represents a training example for our ANN.

In each training example, we define a binary flag, $y_t = 0$ or $y_t = 1$, which describes whether there are additional transiting planets with $P > P_{\text{cut}}$ (or “outers”). In principle, *TESS* will not have direct access to this information (except for the rare cases of single transits, which we ignore in this work). Whilst y_t is not directly measured with *TESS*, our ANN aims to predict its likely value, based upon other features which *TESS* can observe.

3.2 Features

We have some flexibility in how many inputs, or features, we wish to use for the learning. Since we view our work mostly as an initial demonstration of the power of ANNs to this problem, we seek to use a simple set of features rather than performing an exhaustive search.

Guided by this principle, we note that the question we are asking, whether there are *additional* transiting planets, is predicated on the fact there is one or more transiting planets with $P < P_{\text{cut}}$ already known to exist in each training system. Thus, for every training example, we always have information relating to one or more pre-discovered short-period transits. The most basic parameters inferred from a transit are the orbital period, P , and the planetary radius, R , making features related to these terms obvious candidates for our ANN.

We consider the log of each of these variables as potential features, since they are observed to be more smoothly distributed versus linear space (Foreman-Mackey et al. 2014). For a system with N_{inner} transiting planets with $P < P_{\text{cut}}$ (or “inners”), there are a number of single valued features that could be constructed using period and radius, such as the mean, minimum, maximum, etc logarithmic period/radius. In Figures 2 & 3, we show the fraction of outers observed as a function of these various candidate features, where the gray line denotes the flat uniform probability of the ensemble training set. The reduced χ^2 deviance (computed using Poisson counting errors) of these fractions relative to the naive flat probability, which would be expected for irrelevant features, is shown in the top-right of each panel, which can be treated as a feature importance metric.

As evident from Figure 2, all of the period-like features show similar trends to one another, and this is even more true in the case of the radius-like features in Figure 3. We ultimately elect to use $\log R_{\text{max}}$ as our radius-like feature and $\log P(R_{\text{max}})$ as our period-like feature since they are both amongst the strongest features via the χ^2 metrics, but more importantly because they will generally always be available to us as features, for the following reasons.

Whilst *Kepler* and *TESS* are both sensitive to small planets, *Kepler*’s much larger aperture and staring time per field is expected to give it a greater sensitivity to the smallest sized planets (Sullivan et al. 2015). For this reason, the smallest sized planet in a systems with $N_{\text{inner}} > 1$ may not be detectable by *TESS*, even though it resides in our *Kepler*-derived training set. In contrast, features related to the largest-sized planet will very likely always be available. This is because if *TESS* does not discover the largest-sized transiting planet with $P < 13.7$ d, it will very likely not detect any transiting planets in that system at all, since transit detectability is primarily driven by the size of the planet (Kipping & Sandford 2016). Further more, if no transiting planets are known within $P < P_{\text{cut}}$, then the question we seek to answer, is a known transiter accompanied by additional transiting outers, is invalid since there are no known transits to begin with.

Having established $\log R_{\text{max}}$ and $\log P(R_{\text{max}})$ as being viable and influential features, we briefly considered using other features. Notably, we considered whether the properties of the star itself could affect the probability of outers. Both the stellar effective temperature, T_{eff} , and surface

gravity, $\log g$, appear to have little predictive power with relatively low χ^2 metrics, as shown in Figure 4. Consequently, we did not further consider stellar parameters as potential features.

The final feature we considered was an inner multiplicity flag, which takes the value

$$M_{\text{inner}} = \min(N_{\text{inner}} - 1, 1). \quad (6)$$

This feature clearly has a major influence (see Figure 3), yet again it is a feature that may not always be available to us with *TESS*. Whilst the training set, based on *Kepler*, is sensitive to small planets, *TESS* may miss them and again this feature is not generally robust due to the different sensitivities between the two missions. We therefore initially elect to ignore this feature and adopt a two-feature input pattern of $\log R_{\text{max}}$ and $\log P(R_{\text{max}})$, although we develop a hybrid model to include this feature later in Section 4.

3.3 Cross-Validation

In most applications of ANNs, *cross-validation* plays a critical role in providing confidence in the accuracy and robustness of the ANN’s predictions, as well testing different ANN structures and parameters. The idea behind cross-validation is to simply ignore a fraction of the available input pattern, thereby treating the remaining data as the training set and the excluded data as the validation set. The accuracy, however that is defined, of the ANN when applied to the validation set provides a blind test of the usefulness of the trained net. As described below, our treatment frames cross-validation in terms of how we envisage the ANN would be actually be used, in order to blindly demonstrate its practical benefit.

Recall that our ANN will be used to predict which ostensibly single transiting planets are most likely to harbor additional transiting planets at longer orbital periods. Thus, the real world application of our ANN would be to input the catalog of ~ 1700 transiting planet candidates found by *TESS* and rank-order the most likely targets for subsequent, long-term photometric monitoring. The purpose of our ANN is to optimize follow-up, such that it is unnecessary to follow-up all of the *TESS* candidates but rather some fraction, f , selected by the ANN to most likely maximize the yield of new discoveries. This line of thought provides a clear path to testing the value of our trained ANN with cross-validation.

Cross-validation is performed by only training on 75% of the 1786 training examples comprising the *Kepler* input pattern (see Section 3.1 for details). The remaining 446 training examples are treated as the validation set. After learning has finished on the training set, we pass the validation set through the ANN, which provides the class probabilities of each. We then define some follow-up fraction, f , and after rank-ordering the objects by their class probabilities, pick only the top f -quantile. From this follow-up set, we calculate how many successes (i.e. additional transiting planets) were actually observed, S_{ANN} . We then repeat this same process except the follow-up set is randomly selected, and the number of success is saved as S_{R} . The ratio of these values, \mathcal{R} , provides an estimate of how much better our ANN performs versus random picks, where

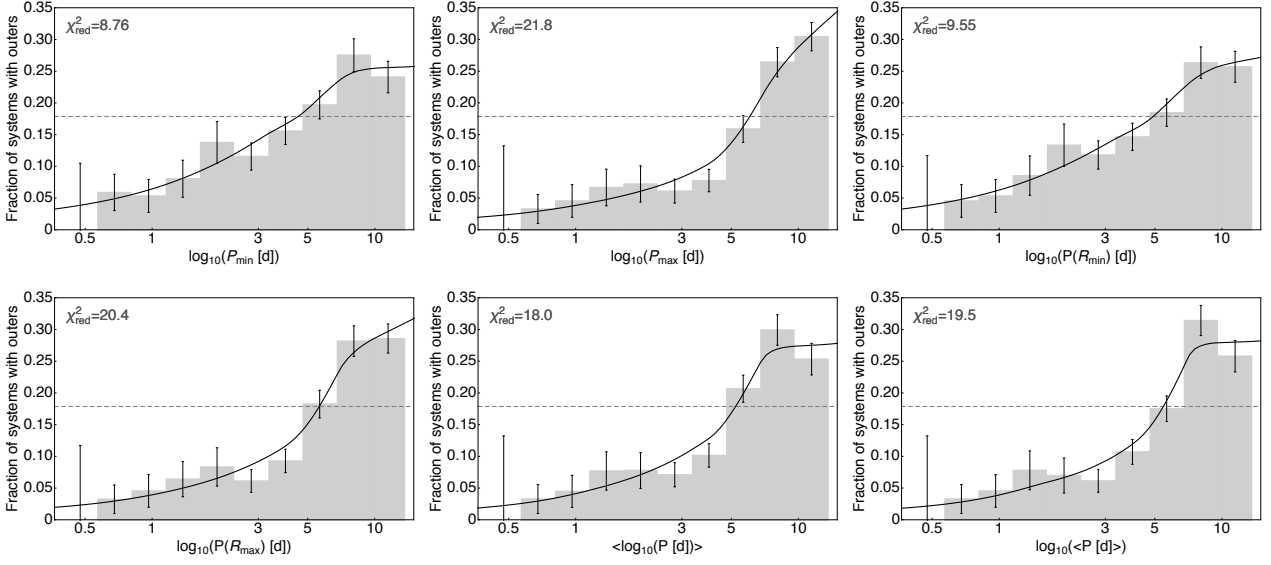


Figure 2. Initial exploration of the predictive power of each period-like feature. Gray dashed horizontal line is the unconditioned a-priori probability of 0.179 ± 0.009 . For comparison, the solid line shows the mean probability predicted by 100 randomly initialized FF ANNs with one hidden layer of four neurons, following the method described in Section 2.

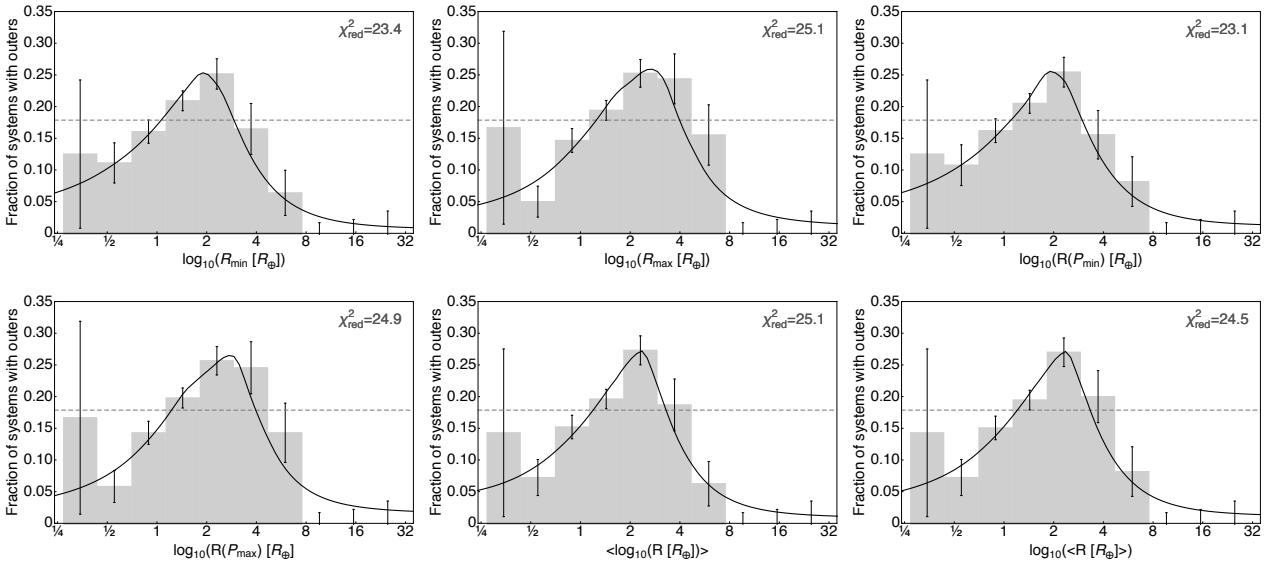


Figure 3. Same as Figure 2, except for radius-like features.

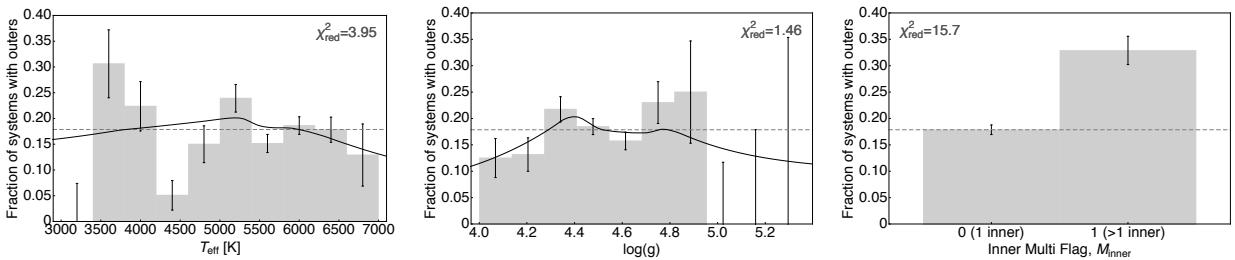


Figure 4. Same as Figure 2, except for three other features related to the system.

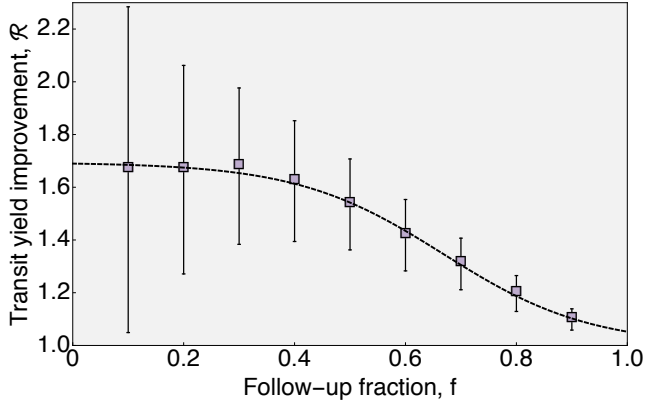


Figure 5. Cross-validation results for our ANN using a single hidden layer of $U = 4$ neurons. We show the ratio of the number of successes achieved by our ANN versus random picks as a function of what fraction of the validation set is followed-up, f . Points represent the median from 10^4 Monte Carlo simulations, the errors represent the 68.3% inter-quantile range and the solid line is a sigmoid fit.

$$\mathcal{R} = S_{\text{ANN}}/S_{\text{R}}. \quad (7)$$

Cross-validation is repeated 10^4 times for any chosen f value. The 10^4 grid comprises of 10^2 randomly sampled validation sets from the full set and 10^2 random initial seeds for the LMA. From the 10^4 estimates of \mathcal{R} , we save the median and 68.3% inter-quantile range as our final estimates. We repeated the whole process for nine choices of f , being 0.1, 0.2, 0.3, 0.4, 0.5, 0.6, 0.7, 0.8 and 0.9. As an example, we show the resulting estimates of \mathcal{R} as a function of f in Figure 5 for a single hidden layer FF ANN with $U = 4$ neurons.

At $f = 0.1$, just 45 validation samples are used, of which only a fraction yield successes, leading to significant Poisson variance. At high f , Poisson variance is suppressed but ultimately in the limit of $f = 1$ any predictor cannot beat random pickings, since rank prioritization no longer has any influence. We generated many example figures like Figure 5 for different numbers of neurons, hidden layers and activation functions and always see the same pattern of \mathcal{R} saturating to some ceiling at $f \sim 0.3$. We find that a logistic sigmoid (solid line in Figure 5) fitted through the cross-validation results may be used to estimate

$$\mathcal{R}_0 \equiv \lim_{f \rightarrow 0} \mathcal{R}, \quad (8)$$

which provides a single-valued metric to assess the cross-validation results in what follows.

3.4 Early Stopping

Properties of the FF ANN, in particular the number of hidden layers and number of neurons, must be chosen. In general, one aims to use the simplest ANN which can accurately relate the output pattern to the input pattern, in or-

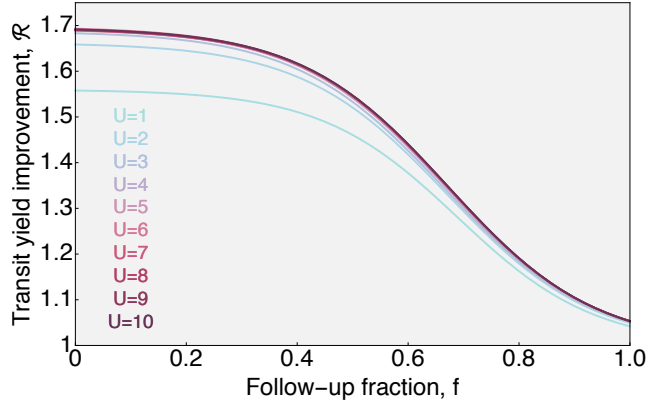


Figure 6. Cross-validation results from ten different single-layer FF ANNs, similar to Figure 5 except we only show the fitted sigmoid. Using early stopping, we identify that cross-validation performance does not improve for $U > 4$ and thus identify this as our preferred ANN.

der to avoid overfitting and for computational expedience. One popular method for choosing the ANN architecture is known as *early stopping*, which we use in this work. Essentially, the objective is to start from a simple model and build up in complexity, stopping once the performance of cross-validation no longer improves.

Here, we start with a single-layer $U = 1$ neuron FF ANN as our simplest model, for which we find $\mathcal{R}_0 = 1.56$. The performance of even this very simple ANN is impressive, yet notably lower than the ~ 1.7 value achieved with the single-layer $U = 4$ ANN shown in Figure 5. Increasing U up to 10, we find no improvement beyond $U = 4$, which is evident from Figure 6. Accordingly, we identify this model as our preferred ANN, for which $\mathcal{R}_0 = 1.69$.

We repeated this exercise using a logistic sigmoid activation function instead of the rectified linear function and find nearly identical results. We also tried using a dual-layer network, exploring a variety of neuron combinations up to a maximum complexity of $U_1 = 6$ and $U_2 = 6$, but find \mathcal{R}_0 does not improve beyond $\simeq 170\%$. As a final test, we trained a triple-layer network with $U_1 = 10$, $U_2 = 8$ and $U_3 = 6$ and similarly found $\mathcal{R}_0 = 1.70$. These results imply that a single-layer $U_1 = 4$ ANN is sufficient to capture the predictive power of the selected features.

4 HYBRID ANN

4.1 Multiple Inners Sample

Of the full training set of 1786 systems, 307 (17%) have multiple transiting planets with $P < P_{\text{cut}}$. Whereas the ensemble sample has a mean probability of hosting additional outers of $17.9 \pm 0.9\%$, this subset has a much higher probability of $33 \pm 3\%$ (as also shown in the right panel of Figure 4). In principle then, this multiplicity feature has a major influence on the class probability. But, as explained in Section 3.2, whilst the positive value of this feature could be obviously

detected by *TESS*, the negative value cannot be ruled out, since *TESS*'s sensitivity is expected to be generally less sensitive to small planets than *Kepler*.

Nevertheless, if multiple inners are detected, the class probability of outer transitters is enhanced and can be calculated with an ANN. We therefore considered an additional ANN trained on three features, where the first two are the same as before but the third is the multiplicity flag, M_{inner} .

4.2 Cross-Validation

To cross-validate, we again emulate the practical way we envisage our trained network being used. If a system is observed to have just one inner, we will predict the class probabilities using the two-feature ANN from before, thereby ignoring the inner multiplicity feature. The logic here is that these systems may indeed have multiple inners, we just don't know it due to *TESS*'s sensitivity bias, and thus we train on the ensemble set. If a system is observed to have multiple inners by *TESS*, then this would also be true as observed in the training set derived from *Kepler*. Accordingly, for these instances we predict the class probability using an ANN trained using the previously described three feature model.

Cross-validation is therefore identical to before except the output to the network (and equivalently for the class probabilities) are now computed using:

$$\hat{y}_i = (1 - M_{\text{inner}})\hat{y}_i^{\text{ANN2}} + M_{\text{inner}}\hat{y}_i^{\text{ANN3}}, \quad (9)$$

where M_{inner} was defined earlier in Equation 6, and the superscripts ANN2 & ANN3 denote the 2- and 3-feature ANN respectively. We may now train ANN2 and ANN3 on a given training set, then use Equation 9 to predict the class probabilities on the associated validation set.

In this way, we have constructed a hybrid of ANN2 and ANN3, which can be also be thought of as a single ANN with a second hidden layer, comprising of \hat{y}_i^{ANN2} and \hat{y}_i^{ANN3} , and a first hidden layer which has numerous synaptic strengths fixed to zero. The hybrid ANN structure is depicted in Figure 7.

4.3 Early Stopping

As before, we use early stopping to identify the simplest possible ANN which maximally improves the yield of transit surveys, described by parameter \mathcal{R}_0 . However, rather than varying the architectures of both ANN2 and ANN3 simultaneously, we fix ANN2 to the $U = 4$ neuron preferred model found earlier and explore single-layer, variable U architectures for ANN3.

As shown in Figure 8, the cross-validation results do not improve beyond $U = 4$ and thus we select the four neuron architecture as the preferred structure. Unlike the two-feature ANN, the cross-validation results display a steep change in \mathcal{R} at $f \sim 0.17$, except for the case of $U = 1$ which again appears smooth. We model the results using two logistic sigmoids, extending upon the single logistic sigmoid used earlier in Section 3.3.

As mentioned at the start of Section 4.1, 17% of the full training set have $M_{\text{inner}} = 1$. Further, as evident from

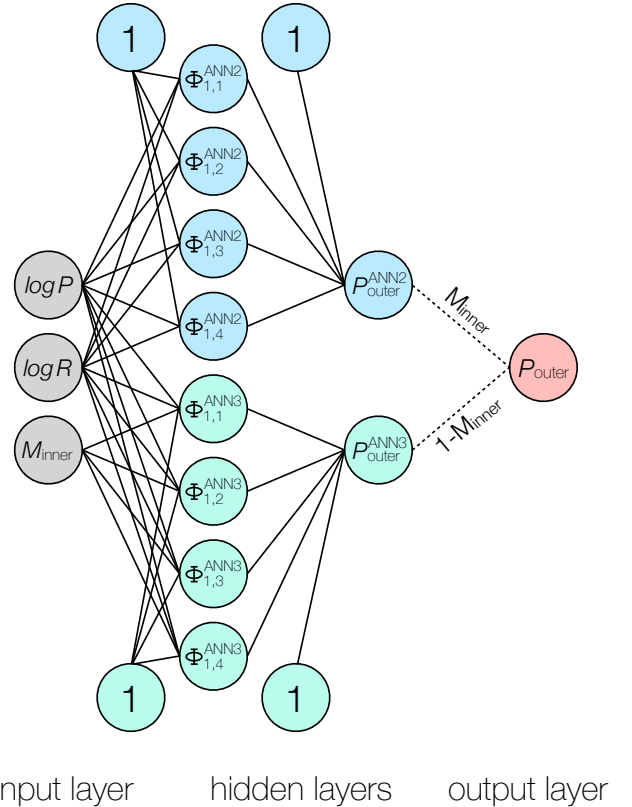


Figure 7. Architecture of our final network, which can be considered as being a hybrid of two single-layer ANNs or one dual-layer ANN with several synaptic strengths fixed to zero.

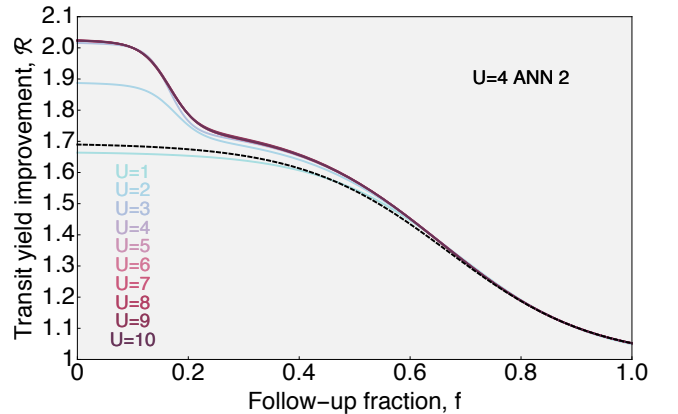


Figure 8. Cross-validation results from our hybrid 2/3-feature ANN, similar to Figure 5 except we only show the fitted sigmoids. Using early stopping, we identify that cross-validation performance stabilizes for $U \geq 4$ and thus identify this as our preferred ANN. For comparison, the black dashed line shows the optimal $U = 4$ ANN when T_{eff} is not used, as found earlier in Section 3.4.

Figure 4, these samples are nearly twice as likely to harbor additional transiting outliers. Therefore, the act of ranking the samples from highest to lowest class probabilities and then selecting the best $f = 0.2$ quantile essentially defines a sample dominated by $M_{\text{inner}} = 1$ cases. The class probability is high for these cases, but once we cross into $f \gtrsim 0.2$, the top quantile starts to include $M_{\text{inner}} = 0$ samples, which have substantially lower class probabilities. This provides an explanation for the steep changes observed in the cross-validation results of Figure 8.

5 INCLUDING EFFECTIVE TEMPERATURE

5.1 Overview

The hybrid ANN discussed in the previous section accounts for three features, a radius-like feature (R_{max}), a radius-like feature ($P(R_{\text{max}})$) and the inner multiplicity flag (M_{inner}). The feature selection was motivated by the feature exploration conducted in Section 3.2 where properties relating to the star, namely T_{eff} and $\log g$, appeared to have little influence on the class probability of an outer. Despite this, there are reasons to revisit this choice.

In what follows, we focus on the feature T_{eff} since it displays a higher χ^2 than $\log g$ in the feature exploration conducted earlier. Since giants have been removed from our sample, T_{eff} and $\log g$ both track the spectral type of the parent star and thus physically speaking are proxies of the same thing.

The lack of a strong χ^2 in Figure 4 for T_{eff} does not necessarily imply it has no predictive power. Correlations with other features could conspire together to mask the effect in a 1D marginalized format, such as that presented in Figure 4. Moreover, it has been established in previous works that the architectures of planetary systems do vary as a function of spectral type (for example see [Mulders et al. 2015](#); [Dressing & Charbonneau 2015](#)). However, we point out that these differences do not necessarily require that the specific output we train upon, class probability of additional transiting planet beyond $P > 13.7$ days, will be substantially distinct.

5.2 Simple Three-Feature ANN

We decided to investigate whether including T_{eff} as an additional feature improves the results of our ANN. We begin by taking the simpler (non-hybrid) ANN described in Section 3, which has just two features (R_{max} & $P(R_{\text{max}})$) and augmenting it with a third feature, T_{eff} . Since the optimal architecture for the ANN cannot be assumed to be the same as that of the previous two-feature case, we repeated the exercise described in Section 3.4 of comparing the cross-validation detection yield improvement factor, \mathcal{R}_0 , for different ANN architectures.

Using a single-layer network, we varied U from 1 to 10 and compared the \mathcal{R} factors, as before. Unlike the two-feature case, the cross-validation results improve up to $U = 4$ (as shown in Figure 9) but then start to worsen beyond that beyond, which implies we are starting to fit out noise which of course has no predictive power.

Figure 9 also reveals that including the third feature

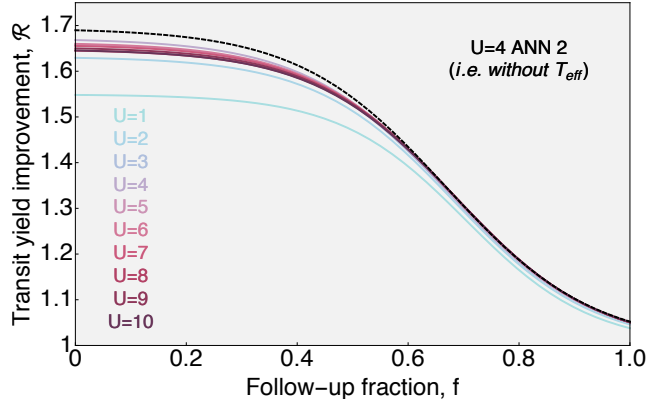


Figure 9. Same as Figure 6, except the single-layer FF ANN now includes an additional feature, T_{eff} . Cross-validation actually degrades for networks using more than 4 neurons, indicating the training is fitting out noise beyond this point. For comparison, the black dashed line shows the optimal $U = 4$ ANN when T_{eff} is not used, as found earlier in Section 3.4.

does not include the cross-validation results, in fact it actually degrades them. For example, the $U = 4$ two-feature network gives $\mathcal{R}_0 = 1.690$ whereas the $U = 4$ three-feature network gives $\mathcal{R}_0 = 1.668$. We considered that perhaps this could be because the network is not complex enough and thus tried using a $U = 36$ single-layer network which gives $\mathcal{R}_0 = 1.678$, indicating that although the predictions seem to improve somewhat from the trend seen in $U = 5 \rightarrow 10$, a single-layer ANN using T_{eff} is not able to recover a prediction as accurate as the simple two-feature ANN can.

As before, we also investigated whether a dual-layer ANN could improve the results and investigated all 36 combinations of U_1 & U_2 from 1 to 6 (i.e. 36 total architectures). The best results were found for the $U_1 = 4$ and $U_2 = 5$ network with $\mathcal{R}_0 = 1.669$, which again is inferior even the single-layer two-feature model for $U = 4$. These results strongly support the result of the earlier exploratory exercise that T_{eff} is not an influential feature in predicting the existence of outliers.

5.3 Hybrid Four-Feature ANN

To confirm this hypothesis, we also tried using the hybrid network described in Section 4 but adding in T_{eff} as an extra feature once again. Since the previous subsection has established that the three-feature component of the hybrid model is optimized for $U = 4$, we kept this part of the network fixed and explored different architectures for the component including M_{inner} , as before.

As was found earlier, increasing U beyond $U = 4$ for this augmented network did not lead to any further improvements in the cross-validation results. Once again, the inclusion of T_{eff} as an extra feature did not improve the predictions of the hybrid network. The highest \mathcal{R}_0 value achieved was $\mathcal{R}_0 = 2.024$, nearly identical to the value found previously when T_{eff} was not included in Section 4 ($\mathcal{R}_0 = 2.024$).

From these results, we conclude that T_{eff} is not a useful feature for predicting the existence of outer transiting planets in known transiting systems with $P < 13.7$ d. In all tests, networks without T_{eff} perform as well or better than those which include it. We stress that this result should not be interpreted as evidence that there are no significant differences between the architectures of planets orbiting stars of differing spectral types. Rather, it only speaks directly to the predictive power of this very specific output that we have defined.

6 DISCUSSION

6.1 Transit Clairvoyance

In this work, we have demonstrated how artificial neural networks (ANNs) may be used to predict which ostensibly single-planet short-period transiting systems are most likely to harbor additional longer-period transiting planets. Focussing on the upcoming *TESS* mission (Ricker et al. 2015), for which in most fields the longest period transits will be 13.7 days (Sullivan et al. 2015), we show how follow-up photometric monitoring for additional transits can expect to have the survey yield improved by a factor of two using our ANN (see Section 4.3).

Although *TESS* fields near the ecliptic pole overlap, permitting for longer-period transit detections, the three-quarters of the survey fields limited to 13.7 day periods severely affects the ability of *TESS* to detect cooler, habitable-zone worlds. From our ANN, we find that some of the short-period transits have up to a 52% probability of hosting an additional longer-period transiting planet (see Figure 11) though, providing an excellent opportunity to increase the science yield of *TESS* and discover many more habitable-zone planets through ANN-guided targeted photometric follow-up from either the ground (e.g. HAT & HAT-S, Bakos et al. 2004, 2013; KELT & KELT-S, Pepper et al. 2004, 2012; MEarth & MEarth-S, Irwin et al. 2009, 2015; NGTS, Wheatley et al. 2013; MINERVA, Swift et al. 2014) or space (e.g. MOST, Croll et al. 2007; CHEOPS, Broeg et al. 2013).

Detecting long-period transiting planets from the ground is challenging, due to the limited ~ 8 hour nightly observing windows. Ground-based networks with longitudinal coverage, such as LCOGT (Brown et al. 2013), are designed to partially remedy this issue though. Naturally, the aforementioned space-based observatories do not suffer this limitation either. Perhaps, though, the most fruitful follow-up program of these predicted planet would not with photometry but via doppler spectroscopy. Here, the fact the outer planet is expected to be transiting maximizes the $m \sin i$ radial velocity amplitude yet observations would not have to be precisely timed to the transit windows. Even a few sparse radial velocity points would be sufficient to both confirm the presence of the planet and greatly narrow-down the likely transit window, paving the way for a subsequent photometric detection.

Our approach should complement the alternative strategies of following up *TESS* single transit events (Yee & Gaudi 2008) and/or scheduling optimized follow up of light curves which display no transits (Dzigan & Zucker 2011). In the

case of single events, long-period planets may fortuitously transit once during the $B = 13.7$ day observing windows, with a probability given by P/B . Our method complements this approach in that certain configurations of inner transiting planet architectures have up to a 50% probability of hosting additional planets, yet may be quite unlikely to display a fortuitous single transit during the observations.

To aid observers planning follow-up using our predictions, we make a grid of the class probabilities with a PYTHON example call available at [this URL](#).

Although our ANN only predicts the binary existence of outers, we can compute an a-posteriori distribution of the period and radius of the innermost outer (which is generally the easiest to blindly detect). To do this, we take the full training data and extract the properties of the minimum period outer, where they exist. The *TESS* target stars do differ from the *Kepler* targets though, in particular the results of Sullivan et al. (2015) show the effective temperature of planet hosting stars will be bimodal, broadly defined as a mixture model with one component resembling the *Kepler* sample and another peak at mid M-dwarfs. If the planet period and radius distribution differs as a function of spectral type, our posterior would be biased. To account for this, we simply exclude the stars in our sample with $T_{\text{eff}} < 4450$ K (although the effect of this is minimal on the posterior). Accordingly, our posterior can be considered as being conditioned on the fact not only an inner is detected but also $T_{\text{eff}} > 4450$ K. Even so, we recommend this posterior only be used as an approximate tool for predicting the parameter space of interest.

The resulting joint posterior is shown in Figure 10, which can be treated as an approximate prediction for the properties of outer planets using our ANN. To summarize, there is an 84% chance of the period being below 50 d with the most likely size being $2.2 R_{\oplus}$.

6.2 *Kepler* vs *TESS*

Our ANN has treated the *Kepler* catalog as the training set, although we envisage the actual application to be on the *TESS* catalog. One might reasonably ask whether there are different sensitivities and biases at play between the two, which may invalidate the results presented here. Although the *TESS* biases are not fully known yet, since the mission has not flown, we argue it is unlikely that the differences between the missions would invalidate the results here, by virtue of how we cognitantly selected our features.

Both missions are essentially photon buckets optimized for approximately visible bandpass photometry and seek planets in the same way. The major differences, in terms of sensitivity, are that i) *Kepler* stared at each star for longer (4.35 yrs versus 27.4 d for most *TESS* stars) ii) *Kepler* has a larger aperture (0.95 m versus 0.127 m) iii) *TESS* will target brighter stars ($V = 4-12$ versus $V = 9-15$). Over the window of $P < 13.7$ d, both missions have nearly continuous photometry and thus the period effect, point i), only serves to increase *Kepler*'s photometric sensitivity by (approximately) the ratio of their baselines square rooted. Points ii) and iii) also both primarily affect the sensitivity to small planets, in opposite directions.

Put together, *Kepler* is expected to have a modestly better sensitivity to small planets (Sullivan et al. 2015), but over

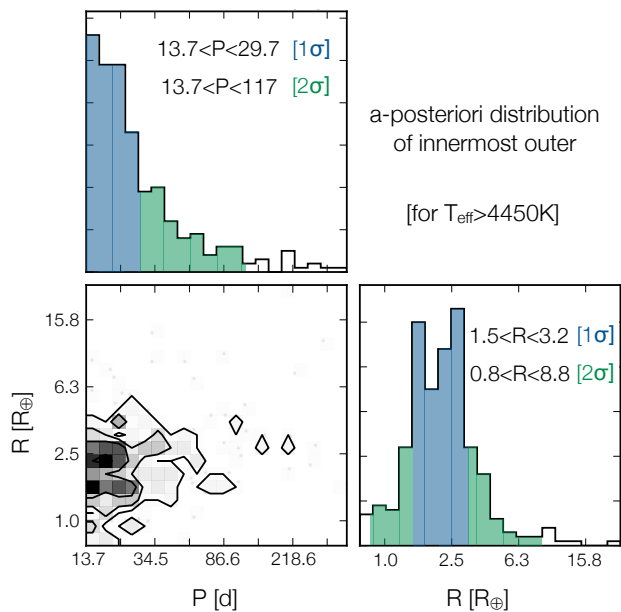


Figure 10. Triangle plot of the a-posteriori probability distribution of the innermost outer transiting planet predicted from our ANN, conditioned on the fact the host star has $T_{\text{eff}} > 4450$ K.

the range of $P < 13.7$ d their detection biases should be very similar, albeit offset. In Section 3.2, we discuss how this insight motivated us to use features related to the largest inner transiting planet only, since *TESS* may not see the smaller objects. If *TESS* does not detect even the largest planet, then one would not be attempted to use our ANN anyway, since the question it poses is predicated on the assumption of at least one known transiting planet.

A final concern we note is with *TESS*'s much greater focus on M-dwarfs than *Kepler*. As studied in detail in Section 5, we are unable to find any indication that the class probability of an inner having an outer is at all influenced by T_{eff} . Since giants were already excluded in our training set, then this indicates that the class probability of interest is no different for M-dwarfs than for the FGK counterparts. Based off these tests and the available information, we argue that our ANN should be able to successfully increase the follow-up yield of *TESS* as described, unless the underlying planet population properties greatly differ from those observed by *Kepler*.

6.3 Physical Insights

Although the primary objective of this work is to predict which *TESS* systems are most likely to harbor additional transiting planets, we briefly discuss the physical significance of our results here. We begin by visualizing the probability space recovered by the ANN.

In Figure 11, we show the probability of a known short-period transiter having an outer as a function of $\log R_{\text{max}}$ and $\log P(R_{\text{max}})$, as computed by our preferred two-feature ANN, ANN2 (see middle panel). Specifically, ANN2 is trained on the entire training set using our preferred structure (single-layer, four neurons; see Section 3.4) and the probabilities

are averaged from 10^3 random initial seedings of the LMA learning algorithm. We make a grid of these results available online at [this URL](#), which may be interpolated for arbitrary inputs. For comparison, we show the case of using a single-neuron ANN in the right panel, which we find has inadequate flexibility. By binning the input data onto a 10 by 10 grid, we can compare the results of the ANN to the solution which it tried to learn (left panel).

Figure 11 reveals a fairly monotonic probability space, with a peak at long orbital periods and intermediate radii. We argue here that the patterns observed at small R are plausibly, although not unequivocally, a result of the sensitivity drop-off of *Kepler* in this region.

Firstly, *Kepler* is known to have significant incompleteness for planets of $R \lesssim 2 R_{\oplus}$ (Christiansen et al. 2016). Second, even perfect transit surveys have lower sensitivity to long-period transits (Kipping & Sandford 2016) and in practice *Kepler*'s sensitivity to long-periods drops even worse than this (Christiansen et al. 2016). Put together, this means that the class probabilities at low R can be lower than the truth, for certain plausible planet populations. For example, if small inner planets tend to be accompanied by approximately equal sized (or smaller) planets at longer periods, then whilst the inner one can be marginally detected by *Kepler*, the outer would evade detection despite its existence. This is compatible with inferences made about the *Kepler* population; in particular Ciardi et al. (2013) find that for planets of $R \lesssim 3 R_{\oplus}$, there is no correlation between the size and location of planets within a multiple transiting planet system.

In contrast, the drop off from intermediate to large planetary radii is likely a real effect since completeness is very high here and only increases with greater R . Jupiter-sized planets with periods below $P < 13.7$ d are usually considered to have migrated from beyond the snow-line (Lin et al. 1996), likely disrupting the planetary system as they go (Steffen et al. 2012; Huang et al. 2016). These hot-Jupiters may therefore have either misaligned the other planets, such that they don't transit, or dynamically ejected them from the system. This picture is supported by the general trend seen in period space, where the shortest period planets rarely haveouters.

In Figure 12, we visualize the probability space again but for the three-feature ANN, ANN3, in the case of $M_{\text{inner}} = 1$. Since the output of ANN3 has zero-weight when $M_{\text{inner}} = 0$ (see Equation 9) in our hybrid network, those results have no bearing on this work and thus are not shown. The ANN3 $M_{\text{inner}} = 1$ class probabilities are generally higher than that of ANN2, which is to be expected based on the earlier feature investigations shown in Figure 4. Additionally, the probability space is more uniform, likely as a result of much sparser set of samples (recall that just 307 of the 1786 training samples have $M_{\text{inner}} = 1$). However, there is a general preference for high $\log P(R_{\text{max}})$, suggesting that ultra compact systems are less likely to have long-period transiting companions.

Together, these results are generally compatible with previously reported trends in the *Kepler* data, but we codify these trends with an ANN to enable quantitative predictions. This work provides one simple example application of ANNs in exoplanetary science (see Waldmann 2016 for another recent example) and we hope this introduction will motivate further applications of this powerful machine learning technique to other problems in the future.

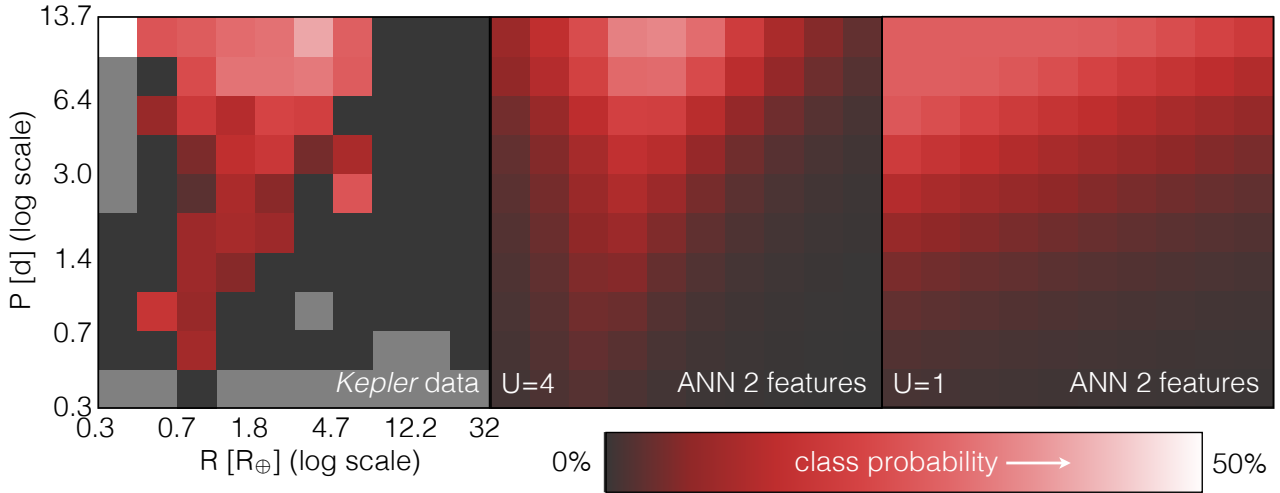


Figure 11. *Left:* Fraction of short-period transitters with long-period transiting companions, as observed in the *Kepler* catalog and binned onto a 10 by 10 grid. Gray squares denote no data. *Middle:* Class probabilities predicted by our preferred two-feature ANN (ANN2) with $U = 4$ neurons, binned into the same space for a fair comparison. *Right:* Same as middle, except using a simpler ANN with just a single neuron.

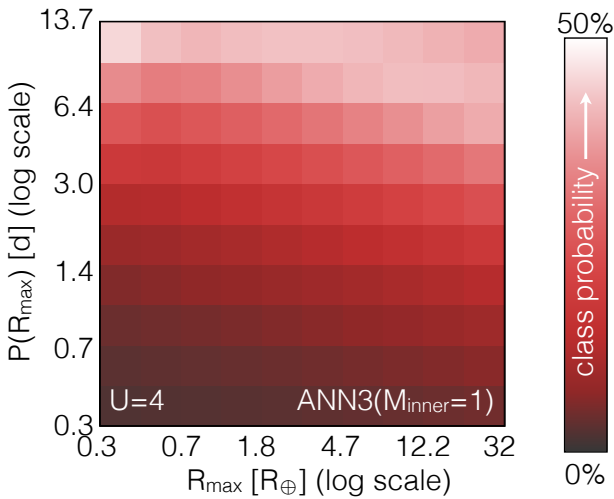


Figure 12. Same as middle panel of Figure 11, except we show the results for the three-feature ANN (ANN3) when $M_{\text{inner}} = 1$. The class probabilities are generally higher when more than one inner is detected and become particularly high when the orbital period of the largest inner is high.

ACKNOWLEDGMENTS

We are grateful to the reviewer for their helpful suggestions and constructive feedback. We thank David Latham, Joshua Pepper, David Charbonneau and the Cool Worlds Lab team for helpful comments and conversations in preparing this manuscript. DMK acknowledges support from NASA grant NNX15AF09G (NASA ADAP Program). This research has made use of the `corner.py` code by Dan Foreman-Mackey at github.com/dfm/corner.py.

REFERENCES

- Akeson, R. L. et al., 2013, *PASP*, 125, 989
 Bailer-Jones, C. A. L., Gupta, R., Singh, H. P., 2001, “An introduction to artificial neural networks” Proceedings of the Workshop on Automated Data Analysis in Astronomy, IUCAA, Pune, India, October 9-12, 2000
 Bakos, G.; Noyes, R. W., Kovács, G., Stanek, K. Z., Sasselov, D. D. & Domsa, I., 2004, *PASP*, 116, 266
 Bakos, G. Á. et al., 2013, *PASP*, 125, 154
 Bishop C. M., 1995, *Neural Networks for Pattern Recognition*, Oxford University Press
 Broeg, C. et al., 2013, *EPJWC*, 47, 3005
 Brown, T. M. et al., 2013, *PASP*, 125, 1031
 Burke, C. J. et al., 2015, *ApJ*, 809, 8
 Christiansen, J. L. et al., 2016, *ApJ*, accepted
 Chen, J. & Kipping, D. M., 2016, submitted
 Ciardi, D. R., Fabrycky, D. C., Ford, E. B., Gautier, T. N., Howell, S. B., Lissauer, J. J., Ragozzine, D. & Rowe, J. F., 2013, *ApJ*, 763, 41
 Coughlin, J. L. et al., 2016, *ApJS*, 224, 12
 Croll, B. et al., 2007, *ApJ*, 658, 1328
 Dong, S. & Zhu, Z., 2013, *ApJ*, 778, 53
 Doyle, L. R. et al., 2011, *Science*, 333, 1602
 Dressing, C. D. & Charbonneau, D., 2015, *ApJ*, 807, 45
 Dzigian, Y. & Zucker, S., 2011, *MNRAS*, 415, 2513
 Foreman-Mackey, D., Hogg, D. W. & Morton, T. D., 2014, *ApJ*, 795, 64
 Graff, P., Feroz, F., Hobson, M. P. & Lasenby, A., 2014, *MNRAS*, 441, 1741
 Haykin, S., 1994, *Neural Networks: A Comprehensive Foundation*, NY: Macmillan.
 Hochrieter, S., 1991, *Untersuchungen zu dynamischen neuronalen Netzen*. Diploma thesis, Institut für Informatik, Technische Univ. Munich
 Howard, A. W. et al., 2012, *ApJS*, 201, 15
 Huang, C. X., Xu, Y. & Triaud, A., 2016, *ApJ*, accepted
 Irwin J. M., Charbonneau, D., Nutzman, P. & Falco, E. E., 2009, in Pont F., Sasselov D., Holman M., eds, *Proc. IAU Symp.* 253, *Transiting Planets*. Cambridge Univ. Press, Cambridge, p. 37
 Irwin, J. M., Berta-Thompson, Z. K., Charbonneau, D.,

- Dittmann, J., Falco, E. E., Newton, E. R.; Nutzman, P., 2015, in Cambridge Workshop on Cool Stars, Stellar Systems, and the Sun, Vol. 18, ed. G. T. van Belle, & H. C. Harris, 767
- Kipping, D. M. & Spiegel, D. S., 2011, MNRAS, 417, L88
- Kipping, D. M. & Sandford, E., 2016, submitted
- LeCun, Y., Bengio, Y. & Hinton, G., 2015, Nature, 521, 436
- Levenberg, K., 1944, Quarterly of Applied Mathematics, 2, 164
- Lin, D. N. C., Bodenheimer, P. & Richardson, D. C., 1996, Nature, 380, 606
- Lundstedt, H. & Wintoft, P., 1994, AnGeo, 12, 19
- Marquardt, D., 1963, SIAM Journal on Applied Mathematics, 11, 431
- Muirhead, P. S. et al., 2012, ApJ, 747, 144
- Mulders, G. D., Pascucci, I. & Apai, D., 2015, ApJ, 814, 130
- Pepper, J. G., Gould, A. & Depy, D. L., 2004, AIPC, 713, 185
- Pepper, J. G., Kuhn, R. B., Siverd, R., James, D. & Stassun, K., 2012, PASP, 124, 230
- Petigura, E. A., Marcy, G. W. & Howard, A. W., 2013, ApJ, 770, 69
- Rappaport, S. et al., 2012, ApJ, 752, 1
- Ricker, G. R. et al., 2015, SPIE Journal of Astronomical Telescopes, Instruments, and Systems, 1, 014003
- Sarle, W. S., 1995, “Stopped Training and Other Remedies for Over-fitting”, Proceedings of the 27th Symposium on the Interface of Computing Science and Statistics, 352-360
- Sliski, D. H. & Kipping, D. M., 2014, ApJ, 788, 148
- Snider, S., Allende Prieto, C., von Hippel, T., Beers, T. C., Sneider, C., Qu, Y. & Rossi, S., 2001, ApJ, 562, 528
- Steffen, J. H. et al., 2012, PNAS, 109, 7982
- Sullivan, P. W. et al., 2015, ApJ, 809, 77
- Swift, J. S. et al., 2015, JATIS, 1, 027002
- Traub, W. A., 2016, ApJ, submitted (arXiv:1605.02255)
- Vanzella, E., 2004, A&A, 423, 761
- Waldmann, I. P., 2016, ApJ, 820, 107
- Wheatley, P. J., et al. 2013, EPJ Web of Conferences, 47, 13002
- Yee, J. C. & Gaudi, S. B., 2008, ApJ, 688, 616

This paper has been typeset from a $\text{\TeX}/\text{\LaTeX}$ file prepared by the author.